Inorganic Chemistry
Article

*Inorg. Chem.* **2010**, *49*, 8287–8297 **8287**
DOI: 10.1021/ic1008522

# Effect of Five Membered Versus Six Membered Meso-Substituents on Structure and Electronic Properties of Mg(II) Porphyrins: A Combined Experimental and Theoretical Study

**Avijit Ghosh,[†] Shaikh M. Mobin,[†] Roland Fröhlich,[‡] Ray J. Butcher,[§] Dilip K. Maity,[*,∥] and Mangalampalli Ravikanth[*,†]**

[†] *Department of Chemistry, Indian Institute of Technology, Bombay, Powai, Mumbai 400 076, India,*
[‡] *Organisch-Chemisches Institut, Universität Münster, Correnssstrasse 40, 48149 Münster, Germany,*
[§] *Department of Chemistry, Howard University, 525 College Street Nw, Washington, D.C. 20059, and*
[∥] *Theoretical Chemistry Section, Chemistry Group, Bhabha Atomic Research Centre, Mumbai 400085, India*

Received April 29, 2010

*Meso*-tetrasubstituted Mg(II) porphyrins containing six membered phenyl groups (MgTPP) and five membered thienyl (MgTThP) and furyl groups (MgTFP) were synthesized and structurally characterized, and the effects of *meso*-substituents on electronic properties were studied using NMR, absorption, fluorescence spectroscopy, and electrochemical studies. Density functional theory (DFT) calculations were carried out to correlate with experimental observations. The three Mg(II) porphyrins MgTPP, MgTThP, and MgTFP were crystallized as hexa-coordinate systems with Mg(II) ion in the center of the porphyrin plane and having two tetrahydrofuran molecules as axial ligands. The X-ray studies clearly showed that the *meso*-furyl groups adopt a conformation in which they are more in-plane with the porphyrin plane whereas the thienyl and phenyl groups prefer an orthogonal arrangement with respect to the porphyrin plane. This arrangement of *meso*-substituents with the porphyrin plane helps in the enhancement of porphyrin $\pi$-delocalization in MgTFP compared to MgTThP and MgTPP. The differences in their structures are clearly reflected in their spectral and electrochemical properties. The absorption and fluorescence bands experienced bathochromic shifts on moving from six membered phenyls to five membered thienyl and furyl group, and the maximum effects were observed for *meso*-tetrafuryl Mg(II) porphyrin. The electrochemical studies indicated that the gap between the highest occupied molecular orbital (HOMO) and the lowest unoccupied molecular orbital (LUMO) decreases as we move from six membered phenyl groups to five membered thienyl and furyl groups, which explains the bathochromic shifts observed in absorption and fluorescence bands. Results on structure and electronic properties based on DFT studies are in agreement with experimental observations.

## Introduction

Magnesium(II) ion is present as centrally coordinated metal in chlorophyll and bacteriochlorophyll and plays a very important role in photosynthesis.[1] Because of their importance in biology, the study of magnesium containing porphyrinic compounds has been of long-standing interest. Magnesium porphyrins are fluorescent compounds bearing a diamagnetic metal ion of ionic radius about 0.72 Å in the porphyrin cavity.[2] Although both zinc and magnesium porphyrins display quite similar absorption and emission properties, magnesium porphyrins exhibit higher fluorescence quantum yields and longer excited state lifetimes (8−10 ns) compared to zinc porphyrins (2−2.5 ns).[3] Importantly, magnesium porphyrins are easier to oxidize by over 250 mV because of the less electronegative magnesium.[4] These interesting electrochemical and photophysical properties of Mg(II) porphyrins have been utilized recently to prepare novel porphyrin dyads[5] and materials for optoelectronic

---

*To whom correspondence should be addressed. E-mail: dkmaity@barc.gov.in (D.K.M.), ravikanth@chem.iitb.ac.in (M.R.). Fax: +91-22-25767152 (M.R.). Phone: +91-22 25767176 (M.R.).

(1) (a) *The Photosynthetic Bacteria*; Clayton, R. K., Sistrom, W. R., Eds.; Plenum Press: New York, 1978. (b) Deisenhofer, J.; Michel, H. *Science* **1989**, *245*, 1463–1473.

(2) (a) Greenwood, N. N.; Earnshaw, A. *Chemistry of the Elements*; Pergamon: Oxford, 1984. (b) Li, F.; Gentemann, S.; Kalsbeck, W. A.; Seth, J.; Lindsey, J. S.; Holten, D.; Bocian, D. F. *J. Mater. Chem.* **1997**, *7*, 1245–1262.

(3) (a) Dorough, G. D.; Miller, J. R.; Huennekens, F. M. *J. Am. Chem. Soc.* **1951**, *73*, 4315–4320. (b) Allison, J. B.; Becker, R. S. *J. Chem. Phys.* **1960**, *32*, 1410–1417.

(4) Kadish, K. M.; Van Caemelbecke, E.; Royal, G. In *The Porphyrin Handbook*; Kadish, K. M., Smith, K. M., Guilard, R., Eds.; Academic Press: New York, 2000; Vol. *8*, Chapter 55, pp 1−114.

(5) (a) Zaleski, J. M.; Chang, C. K.; Leroi, G. E.; Cukier, R. I.; Nocera, D. G. *J. Am. Chem. Soc.* **1992**, *114*, 3564–3465. (b) Wynne, K.; LeCours, S. J.; Galli, C.; Therien, M. J.; Hochstrasser, R. M. *J. Am. Chem. Soc.* **1995**, *117*, 3749–3753. (c) Li, J.; Diers, J. R.; Seth, J.; Yang, S. I.; Bocian, D. F.; Holten, D.; Lindsey, J. S. *J. Org. Chem.* **1999**, *64*, 9090–9100. (d) Natan, M. J.; Hoffman, B. M. *J. Am. Chem. Soc.* **1989**, *111*, 6468–6470. (e) Hascoat, P.; Yang, S. I.; Lammi, R. K.; Alley, J.; Bocian, D. F.; Lindsey, J. S.; Holten, D. *Inorg. Chem.* **1999**, *38*, 4849–4853.

device applications.[6] Generally, the magnesium(II) porphyrins were prepared under harsh conditions by treating porphyrin with $MgX_2$ (X = Cl and Br) in refluxing dimethylformamide (DMF).[7] Lindsey and co-workers[8] recently developed simple homogeneous and heterogeneous methods at room temperature for insertion of Mg(II) ion into the porphyrin and related macrocycles. There are several reports on structurally characterized Mg(II) porphyrins where their ground and excited state dynamics have been studied, but these reports are restricted to Mg(II) porphyrins having six membered aryl groups such as phenyls or substituted phenyls or pyridyls at *meso*-positions.[9] Recently, we and others have synthesized *meso*-aryl porphyrins having five membered aryl groups such as furyls, thienyls, pyrazolyls, imidazoles, pyrrolyls, or azulenyls at *meso*-positions.[10] The limited studies available in the literature clearly showed that the electronic properties of the porphyrin ring are greatly altered when six membered *meso*-aryl groups are replaced with five membered aromatic heterocycles. A perusal of the literature reveals that metalloporphyrin chemistry with five membered *meso*-substituents has remained largely unexplored,[11] and to the best of our knowledge, there is no systematic study on the structure and electronic properties of tetraryl substituted metalloporphyrins having six membered aryl groups versus five membered aryl groups as *meso*-aryl substituents. In this paper, we report the synthesis, structure, optical, electrochemical, and fluorescence properties of Mg(II) porphyrins having six membered phenyl groups as well as Mg(II) porphyrins having five membered thienyl and furyl groups at *meso*-positions. The study clearly shows that the structure and electronic properties of Mg(II) porphyrins are greatly altered on changing six membered *meso*-phenyls with five membered *meso*-thienyls or *meso*-furyls, and maximum effects were observed with Mg(II) porphyrin having five membered furyl groups at *meso*-positions. To support the inferences drawn based on experimental results and to provide more insight into the effect of substituents on electronic properties of these Mg(II) porphyrins, quantum chemical calculations were carried out applying density functional theory (DFT). Despite their immense importance in biology, only a few theoretical studies on Mg-porphyrin systems have been made to study electronic absorption properties of these macrocyclic systems (which are rather large for ab initio calculations).[12,13] In the present study, DFT based equilibrium structures in the ground ($S_0$) state and electronic properties in the ground as well as excited states of these three Mg(II) porphyrins are reported. UV−vis spectra of these systems are simulated based on calculated excited state properties following Time Dependent DFT (TD-DFT). A direct correlation is observed in the shift of absorption maxima ($\lambda_{max}$) between the experimental and theoretical values especially in the Soret band region. Contour plots of frontier orbitals are generated to assign the type of electronic transitions involved. Energy gaps between the highest occupied molecular orbital (HOMO) and the lowest unoccupied molecular orbital (LUMO) are also calculated to see the effect of substituents in tuning the energy gaps in these Mg(II) porphyrinic systems and correlated with the experimental results based on electrochemical studies. Again, a very good correlation is achieved between the experimental and the theoretical values of energy gaps.

## Results and Discussion

There are several methods available to synthesize Mg(II) porphyrins. However the approach adopted by Lindsey et al.,[8] is very simple and gives Mg(II) porphyrins in high yield. We adopted Lindsey's homogeneous approach[8a] to synthesize MgTPP and MgTFP (Scheme 1). According to Lindsey's approach, we reacted the corresponding free base porphyrin in $CH_2Cl_2$ with $MgBr_2 \cdot O(Et)_2$ for 15 min at room temperature. The reaction progress was monitored by UV−visible spectroscopy. Interestingly, the method worked well only for the synthesis of MgTPP and MgTFP (Scheme 1) but did not work for MgTThP. We used the conventional approach to synthesize MgTThP by refluxing $H_2$TThP with excess $MgCl_2$ in DMF[7] (Scheme 1). The compounds MgTPP, MgTThP, and MgTFP were purified by alumina column chromatography and recrystallized from tetrahydrofuran (THF). The formation of Mg(II) porphyrins was confirmed by observation of a molecular ion peak in the mass spectra. The structures of Mg(II) porphyrins were determined by X-ray

---

(6) (a) Ambroise, A.; Wagner, R. W.; Rao, P. D.; Riggs, J. A.; Hascoat, P.; Diers, J. R.; Seth, J.; Lammi, R. K.; Bocian, D. F.; Holten, D.; Lindsey, J. S. *Chem. Mater.* **2001**, *3*, 1023–1034. (b) Wagner, R. W.; Lindsey, J. S.; Seth, J.; Palaniappan, V.; Bocian, D. F. *J. Am. Chem. Soc.* **1996**, *118*, 3996–3997.

(7) Adler, A. D.; Longo, F. R.; Kampas, F.; Kim, J. *J. Inorg. Nucl. Chem.* **1970**, *32*, 2443–2445.

(8) (a) Lindsey, J. S.; Woodford, J. N. *Inorg. Chem.* **1995**, *34*, 1063–1069. (b) O'Shea, D. F.; Miller, M. A.; Matsueda, H.; Lindsey, J. S. *Inorg. Chem.* **1996**, *35*, 7325–7338.

(9) (a) Timkovich, R.; Tulinsky, A. *J. Am. Chem. Soc.* **1969**, *91*, 4430–4432. (b) Byrn, M. P.; Curtis, C. J.; Hsiou, Y.; Khan, S. I.; Sawin, P. A.; Tendick, S. K.; Terzis, A.; Strouse, C. E. *J. Am. Chem. Soc.* **1993**, *115*, 9480–9491. (c) Collins, D. M.; Hoard, J. L. *J. Am. Chem. Soc.* **1970**, *92*, 3761–3771. (d) Storm, C. B.; Corwin, A. H.; Arellano, R. R.; Martz, M.; Weintraub, R. *J. Am. Chem. Soc.* **1966**, *88*, 2525–2531. (e) Fuhrhop, J.-H.; Mauzerall, D. *J. Am. Chem. Soc.* **1969**, *91*, 4174–4181. (f) Proni, G.; Pescitelli, G.; Huang, X.; Nakanishi, K.; Berova, N. *J. Am. Chem. Soc.* **2003**, *125*, 12914–12927. (g) Lintuluoto, J. M.; Borovkov, V. V.; Inoue, Y. *J. Am. Chem. Soc.* **2002**, *124*, 13676–13677. (h) Berg, A.; Rachamim, M.; Galili, T.; Levanon, H. *J. Phys. Chem.* **1996**, *100*, 8791–8795. (i) Kadish, K. M.; Shiue, L. R. *Inorg. Chem.* **1982**, *21*, 1112–1115. (j) Mckee, V.; Rodley, C. A. *Inorg. Chim. Acta* **1988**, *151*, 233–236. (k) Barkigia, K. M.; Spaulding, L. D.; Fajer, J. *Inorg. Chem.* **1983**, *22*, 349–351. (l) Hibbs, W.; Arif, A. M.; Botoshansky, M.; Kaftory, M.; Miller, J. S. *Inorg. Chem.* **2003**, *42*, 2311–2322. (m) McKee, V.; Ong, C. C.; Rodley, G. A. *Inorg. Chem.* **1984**, *23*, 4242–4248. (n) Szulbinski, W. S. *Inorg. Chim. Acta* **1995**, *228*, 243–250. (o) Osuka, A.; Marumo, S.; Taniguchi, S.; Okada, T.; Mataga, N. *Chem. Phys. Lett.* **1994**, *230*, 144–148. (p) Loewe, R. S.; Lammi, R. K.; Diers, J. R.; Kirmaier, C.; Bocian, D. F.; Holten, D.; Lindsey, J. S. *J. Mater. Chem.* **2002**, *12*, 1530–1552. (q) El-Khouly, M. E.; Araki, Y.; Ito, O.; Gadde, S.; McCarty, A. L.; Karr, P. A.; Zandlerb, M. E.; D'Souza, F. *Phys. Chem. Chem. Phys.* **2005**, *7*, 3163–3171. (r) Bonnett, R.; Hursthouse, M. B.; Malik, K. M. A.; Mateen, B. *J. Chem. Soc., Perkin Trans. 2* **1977**, 2072–2076. (s) Atefi, F.; McMurtrie, J. C.; Arnold, D. P. *Dalton Trans.* **2007**, 2163–2170.

(10) (a) Gupta, I.; Ravikanth, M. *Tetrahedron* **2003**, *59*, 6131–6139. (b) Guo, C. C.; Ren, T. G.; Wang, J.; Li, C. Y.; Song, J. X. *J. Porphyrins Phthalocyanines* **2005**, *9*, 430–436. (c) Bhaumik, J.; Yao, Z.; Borbas, K. E.; Taniguchi, M.; Lindsey, J. S. *J. Org. Chem.* **2006**, *71*, 8807–8817. (d) Gupta, I.; Ravikanth, M. *J. Photochem. Photobiol. A:* (*Chem*). **2006**, *177*, 156–163. (e) Kurotobi, K.; Osuka, A. *Org. Lett.* **2005**, *7*, 1055–1058. (f) Furuta, H.; Maeda, H.; Osuka, A. *Org. Lett.* **2000**, *2*, 187–189. (g) Brueckner, C.; Foss, P. C. D.; Sullivan, J. O.; Pelto, R.; Zeller, M.; Birge, R. R.; Crundwell, G. *Phys. Chem. Chem. Phys.* **2006**, *8*, 2402–2412. (h) Santosh, G.; Ravikanth, M. *Chem. Phys. Lett.* **2007**, *448*, 248–252. (i) Santosh, G.; Ravikanth, M. *Tetrahedron* **2007**, *63*, 7833–7844.

(11) (a) Rochford, J.; Botchway, S.; McGarvey, J. J.; Rooney, A. D.; Pryce, M. T. *J. Phys.Chem. A* **2008**, *112*, 11611–11618. (b) Boyle, N. M.; Rochford, J.; Pryce, M. T. *Coord. Chem. Rev.* **2010**, *254*, 77–102. (c) Purushothaman, B.; Varghese, B.; Bhyrappa, P. *Acta Crystallogr. Sect. C: Cryst. Struct. Commun.* **2001**, *C57*, 252–253.

(12) Sundholm, D. *Chem. Phys. Lett.* **2000**, *317*, 392–399.

(13) Rubio, M.; Roos, B. O. *J. Chem. Phys.* **1999**, *110*, 7202–7209.

**Scheme 1.** Synthesis of Mg(II) Porphyrins [MgTPP, MgTThP, and MgTFP]

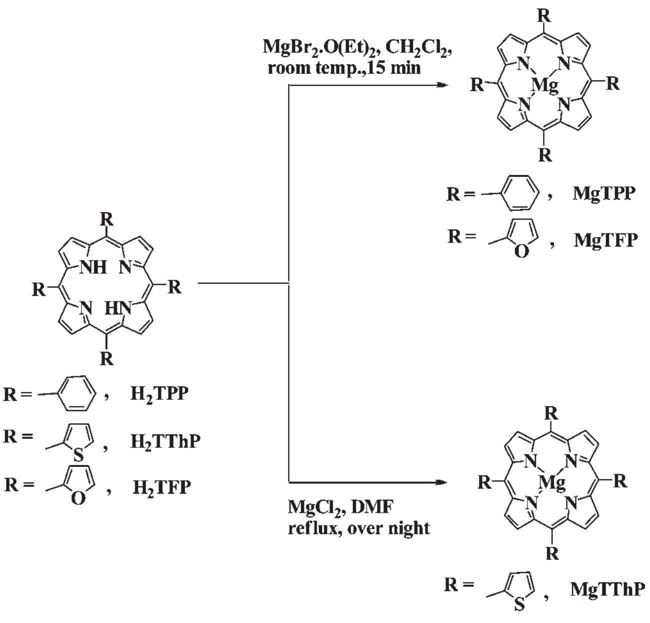

crystallography, and the electronic properties were studied by spectroscopic and electrochemical techniques.

**Crystallographic Characterization of MgTPP, MgTThP, and MgTFP.** All three molecules were crystallized via slow diffusion of *n*-hexane into the THF solutions of Mg(II) porphyrins over a period of one week. The compounds MgTPP and MgTThP were crystallized in the triclinic space group $P\bar{1}$ whereas MgTFP was crystallized in the monoclinic space group $P2_1/c$. The crystal data and data collection parameters are given in Table 1, and comparisons of selected bond distances and bond angles of MgTPP, MgTThP, and MgTFP are given in Table 2. A comparison of perspective views of MgTPP, MgTThP, and MgTFP is shown in Figure 1. All three Mg(II) porphyrin complexes exhibit hexa-coordinated octahedral geometry with two tetrahydrofuran molecules bonded to Mg(II) ion as fifth and sixth ligands (hence these complexes are represented as $Mg(II)P(THF)_2$, where P = TPP, TThP, and TFP). Magnesium porphyrins may crystallize either in five-coordinated or six-coordinated geometric fashion depending on the nature of the solvent used for the crystallization.[9a,j,k,m,14] In five-coordinated entities, the magnesium atom is displaced out of the mean plane of the four pyrrole nitogen atoms toward the axial ligands, by values ranging from 0.027 to 0.496 Å, whereas this out-of-plane displacement of central magnesium atom is negligible in six coordinated cases. In all three Mg(II) porphyrins the central Mg(II) ion is perfectly in the plane defined by four *meso*-carbons as it is located on a crystallographic center of inversion. A comparison of the structures and geometrical features of all complexes is shown in Table 3, and it is clear that there is no out of plane displacement of the central Mg(II) ion and porphyrin nonplanarity is also neligible in all three cases. However, the four pyrrole rings are not coplanar and deviate alternately up and down from the mean plane giving a wave-like conformation. The deviation of pyrrole rings from the mean plane of the four *meso*-carbons of porphyrin helps in the decrease of dihedral angle between porphyrin plane and *meso*-substituents which in turn leads to strong electronic interaction between the porphyrin ring and *meso*-substituents. In $Mg(II)TPP(THF)_2$, $Mg(II)TThP(THF)_2$, and $Mg(II)TFP(THF)_2$, pyrroles A/C and B/D deviate by 8.01°/5.05°, 7.16°/5.51°, and 9.74°/5.10°, respectively.

A close inspection of structures of Mg(II) porphyrins indicates that in the case of MgTPP and MgTThP, one set of *trans meso*-aryl groups are almost perpendicular to the plane of the porphyrin (99.3° and 87.5°, respectively) whereas the dihedral angle for the other set of *meso*-aryl groups is considerably reduced (57.1° and 58.2°, respectively). For MgTFP, on the other hand, not only is the average dihedral angle much smaller than those for both MgTPP and MgTThP but both dihedral angles have similar values (46.3° and 50.8°). This reduced dihedral angle indicates that there is more coplanarity between the *meso*-furyl groups and the porphyrin plane in $Mg(II)TFP(THF)_2$ which helps in the enhancement of $\pi$-conjugation resulting in the observed alteration of its electronic properties. This is also clearly reflected in several bond distances such as $C_\alpha-C_\beta$, $C_\beta-C_\beta$, $C_m-C_{ma}$, and so forth (Figure 2 and Table 2), which are shorter for $Mg(II)TFP(THF)_2$ as compared with the other two Mg(II) porphyrins (Table 2). Furthermore, the axial THF ligands are involved in steric interaction with *meso*-substituents in $Mg(II)TPP(THF)_2$ and $Mg(II)TThP(THF)_2$; hence the axial ligands in these two Mg(II) porphyrins are distorted unlike in $Mg(II)TFP(THF)_2$. This can be due to the orthogonal arrangement of *meso*-aryl groups with respect to porphyrin plane in MgTPP and MgTThP which causes the steric hindrance leading to distortion of THF ligands. However, in MgTFP, the *meso*-furyl groups are more coplanar with the porphyrin leading to less steric hindrance between axial THF ligands and *meso*-furyl groups. This is also reflected in the bond distance between Mg(II) ion and axial "O" of tetrahydrofuran which is longer for $Mg(II)TPP(THF)_2$ and $Mg(II)TThP(THF)_2$ (by ~0.05 Å) and shorter for $Mg(II)TFP(THF)_2$ supporting the observation that the axial ligands can approach Mg(II) ion more closely in $Mg(II)TFP(THF)_2$ because of the equivalent conformation adopted by its *meso*-furyl substituents. The binding properties of central metal ion in these Mg(II) porphyrin complexes are quite different compared to transition metal porphyrin complexes. For the $Fe(II)TPP(THF)_2$ complex,[15] which is quite similar to $Mg(II)TPP(THF)_2$, the average M—N bond lengths are quite comparable with $Mg(II)TPP(THF)_2$ but the M—O distance is considerably longer by ~0.11 Å. This indicates that the axial THF molecules are loosely bound to $Fe(II)TPP(THF)_2$ complex compared to $Mg(II)TFP(THF)_2$ where the M—O distance is shorter and indicates that the axial THF ligand is strongly coordinated to the oxo-philic Mg(II) ion.

---

(14) (a) Fischer, M. S.; Templeton, D. H.; Zalkin, A.; Calvin, M. *J. Am. Chem. Soc.* **1971**, *93*, 2622–2628. (b) Chow, H. C.; Serlin, R.; Strouse, C. E. *J. Am. Chem. Soc.* **1975**, *97*, 7230–7237. (c) Serlin, R.; Chow, H. C.; Strouse, C. E. *J. Am. Chem. Soc.* **1975**, *97*, 7237–7242. (d) Kratky, C.; Dunitz, J. D. *Acta Crystallogr., Sect. B: Struct. Crystallogr. Cryst. Chem.* **1977**, *B33*, 545–547. (e) Kratky, C.; Isenring, H. P.; Dunitz, J. D. *Acta Crystallogr., Sect. B: Struct. Crystallogr. Cryst. Chem.* **1977**, *B33*, 547–549.

(15) Barkigia, K. M.; Palacio, M.; Sun, Y.; Nogues, M.; Renner, M. W.; Varret, F.; Battioni, P.; Mansuy, D.; Fajer, J. *Inorg. Chem.* **2002**, *41*, 5647–5649.

**Table 1.** Crystallographic Data for MgTPP, MgTThP, and MgTFP

| parameters | MgTPP | MgTThP | MgTFP |
|---|---|---|---|
| mol formula | $C_{48}H_{40}MgN_4O_2$ | $C_{44}H_{36}MgN_4O_2S_4$ | $C_{44}H_{36}MgN_4O_6$ |
| fw | 928.89 | 805.32 | 741.08 |
| cryst sym | triclinic | triclinic | monoclinic |
| space group | $P\bar{1}$ | $P\bar{1}$ | $P2_1/c$ |
| $a$ (Å) | 12.3262(18) | 9.5942(7) | 9.882(7) |
| $b$ (Å) | 12.326(3) | 10.1952(7) | 20.508(3) |
| $c$ (Å) | 13.9882(16) | 11.7484(8) | 9.566(4) |
| $\alpha$ (deg) | 98.702(13) | 66.492(3) | 90 |
| $\beta$ (deg) | 105.311(11) | 76.053(3) | 115.24 |
| $\gamma$ (deg) | 95.727(14) | 65.476(6) | 90 |
| $V$ (Å$^3$) | 2004.4(6) | 954.80(12) | 1753.7(14) |
| $Z$ | 2 | 1 | 2 |
| $\mu$ (mm$^{-1}$) | 0.091 | 2.804 | 0.110 |
| $D_{\text{calcd}}$ (g cm$^{-3}$) | 1.267 | 1.401 | 1.403 |
| $F$(000) | 944 | 420 | 776 |
| $2\theta$ range (deg) | 3.08−49.96 | 4.12−67.82 | 3.02−25.00 |
| $e$ data ($R_{\text{int}}$) | 6996/0.0327 | 10709/0.036 | 10800/0.0311 |
| R1, wR2 [$I > 2\sigma(I)$] | 0.0481, 0.1085 | 0.0451, 0.1207 | 0.0353, 0.0905 |
| R1, wR2 (all data) | 0.1292, 0.1307 | 0.0487, 0.1245 | 0.0496, 0.0935 |
| GOF | 1.013 | 1.041 | 1.030 |
| largest diff. peak/hole, (e Å$^{-3}$) | 0.823 /−0.570 | 0.499/−0.333 | 0.709/−0.264 |

**Table 2.** Comparison of Some Selected Bond Length [Å] and Bond Angles [deg] Obtained from Both X-ray Crystal Structure and Optimized Structure

| | X-ray structure | | | optimized structure | | |
|---|---|---|---|---|---|---|
| parameter | MgTPP | MgTThP | MgTFP | MgTPP | MgTThP | MgTFP |
| Mg−N1 | 2.073(1) | 2.073(1) | 2.084(2) | 2.09 | 2.09 | 2.09 |
| Mg−N2 | 2.070(1) | 2.073(1) | 2.077(2) | 2.09 | 2.09 | 2.09 |
| Mg−N3 | 2.073(3) | 2.073(1) | 2.084(2) | 2.09 | 2.09 | 2.09 |
| Mg−N4 | 2.070(1) | 2.073(1) | 2.077(2) | 2.09 | 2.09 | 2.09 |
| Mg−O | 2.241(1) | 2.267(2) | 2.210(2) | 2.28 | 2.27 | 2.27 |
| $C_m-C_{ma}$[a] | 1.493 | 1.488 | 1.473 | 1.49 | 1.48 | 1.47 |
| $C_\beta-C_\beta$[a] | 1.349 | 1.352 | 1.346 | 1.36 | 1.36 | 1.36 |
| $C_\beta-C_\alpha$[a] | 1.442 | 1.444 | 1.444 | 1.44 | 1.44 | 1.44 |
| dihedral angle[b] | 78.2 | 72.8 | 48.5 | 65.9 | 70.3 | 52.9 |

[a] Average bond distance (in Å). [b] Average dihedral angle (deg) between porphyrin ring and *meso*-substituents. $C_m-C_{ma}$ is the average distance (Å) between *meso*-carbon atom and the carbon atom through which respective *meso*-aryl group is attached to *meso*-positions.

In addition to the above-mentioned differences between the structures of Mg(II) TFP(THF)$_2$ and Mg(II)-TPP(THF)$_2$, a novel feature of Mg(II)TFP(THF)$_2$ is the presence of intramolecular and intermolecular hydrogen bonding interactions. The intramolecular hydrogen bonding as shown in the packing diagram (Figure 3) is present between *meso*-furyl "O" and $\beta$-pyrrole "H" which may be assisting in the decrease of dihedral angle between *meso*-furyl groups and plane of the porphyrin. In addition, the Mg(II)TFP(THF)$_2$ also shows intermolecular hydrogen bonding (O2$\cdots\cdot$H−C14 and C14—H$\cdots\cdot$O2) between *meso*-furyl "O" (O2) of one porphyrin unit with "H" (H14) of *meso*-furyl group of second porphyrin and vice versa leading to the formation of the supramolecular assembly (Figure 4). A weak hydrogen bonding is also observed between O2 of *meso*-furyl group and H−C8 of *meso*-furyl group from other porphyrin unit. Thus, MgTFP(THF)$_2$ exhibits different structural properties than other two Mg(II) porphyrins. Note that crystal structures have produced two different sets of dihedral angles between *meso*-groups and porphyrin plane in case of MgTPP and MgTThP as the *meso*-groups are not involved in H−bonding. However, as it was just discussed, there are H−bonds between two macrocyclic porphyrin systems in case of MgTFP supramolecular assembly resulting in all the dihedral angles between *meso*-groups and porphyrin plane being similar as shown in Figure 4 since each unit feels equal interactions.

**Spectral and Electrochemical Properties.** The effect of six membered phenyl groups versus five membered thienyl and furyl groups is clearly reflected in their spectral and electrochemical properties, and these are in agreement with their crystal structures. The comparison of $^1$H NMR spectra of MgTPP, MgTThP, and MgTFP recorded in $CDCl_3$ is presented in Figure 5. In all three Mg(II) porphyrins, the eight $\beta$-pyrrole protons appeared as singlets. However, the $\beta$-pyrrole protons experienced ~0.2 ppm downfield shift on changing the *meso*-substituent from six membered phenyl group to five membered thienyl and furyl groups, and maximum downfield shift was observed for MgTFP. This indicates that there is an alteration in ring current on changing the *meso*-substituent from six membered phenyl group to five membered thienyl and furyl groups. From crystal structures, it is clear that among Mg(II) porphyrins, the *meso*-substituents are more coplanar with the porphyrin plane only in MgTFP, leading to strong interaction between porphyrin macrocycle and *meso*-furyl groups. This interaction results in the alteration of $\pi$-conjugation which results in the more downfield shift of $\beta$-pyrrole protons in MgTFP compared to MgTPP and MgTThP.

Similar observations were made in the absorption spectroscopy. The Q- and Soret band absorption spectra of MgTPP, MgTThP, and MgTFP are shown in Figure 6, and absorption data are presented in Table 4. Inspection of Figure 6 and Table 4 reveals the following: (1) In general, all three Mg(II) porphyrins showed two Q-bands and one strong Soret band; (2) both Soret and Q-bands experienced bathochromic shifts with slight alteration in absorption coefficients on changing six membered phenyl groups with five membered thienyl and furyl groups at *meso*-positions and (3) the maximum red shifts in absorption bands were observed for MgTFP compared to MgTThP. Thus, the absorption study supported the alteration of electronic properties of the Mg(II) porphyrin on changing six membered phenyl groups with five

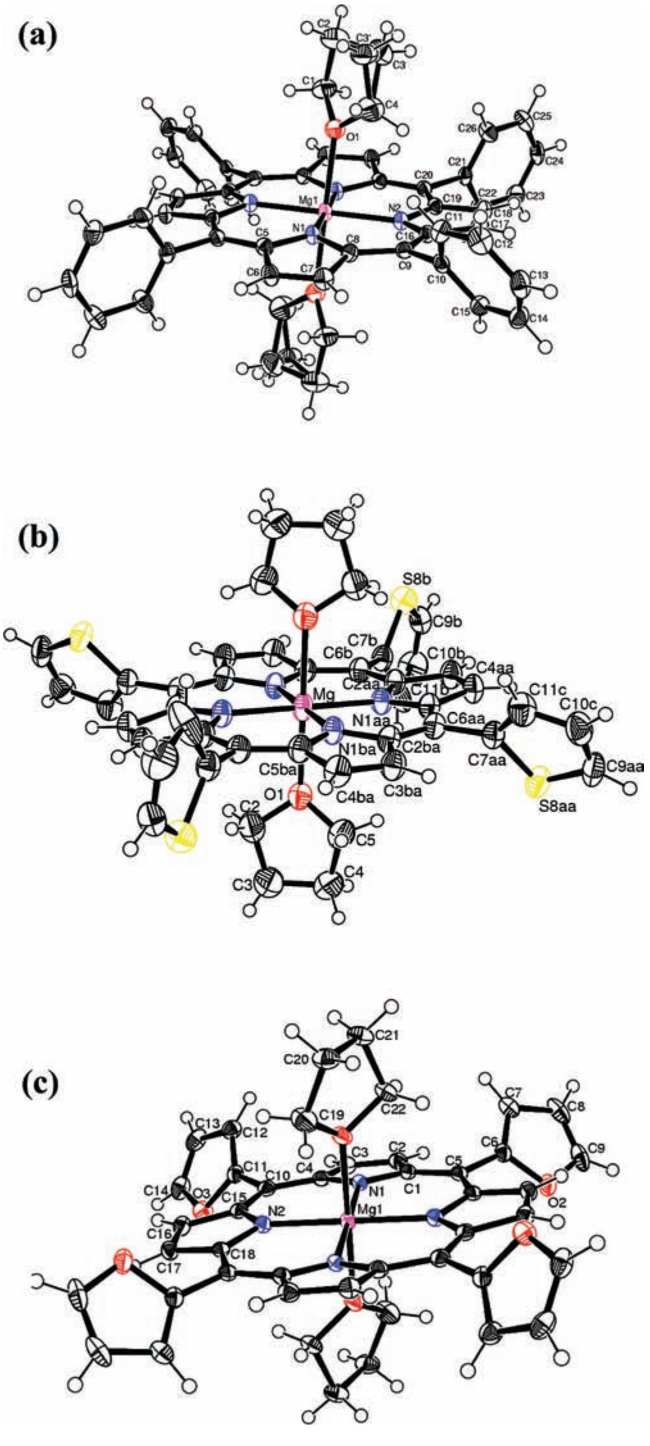

**Figure 1.** ORTEP diagram of compounds (a) MgTPP, (b) MgTThP, and (c) MgTFP. Ellipsoids are drawn at 50% probability level.

membered thienyl and furyl groups at *meso*-positions. These effects are attributed to the orientation of *meso*-substituents with respect to the mean plane of the porphyrin. In MgTPP and MgTThP, the *meso*-substituents are arranged in orthogonal fashion with respect to the mean plane of the porphyrin resulting in the prevention of significant $\pi$-conjugation between porphyrin and *meso*-substituents. However, in MgTFP, the five membered *meso*-furyl groups are more in-plane with the porphyrin ring resulting in efficient extension of the porphyrin $\pi$-conjugation into *meso*-substituents. This is also reflected in our DFT studies of Mg(II) porphyrins which supports more orbital overlap of *meso*-substituents with porphyrin ring in MgTFP. The trends observed in the absorption properties are in agreement with the X-ray structures of MgTPP, MgTThP, and MgTFP.

**Table 3.** Selected Geometrical Parameters

| | MgTPP | MgTFP | MgTThP |
|---|---|---|---|
| $Mg-N_p$ [a,b] | 2.072 | 2.080 | 2.073 |
| $Mg-O_{ax}$ [a,b] | 2.241(12) | 2.210(16) | 2.267(16) |
| $\Delta_{24}^{Mg}$ [c] | 0.00 | 0.00 | 0.00 |
| $\Delta_{4N}^{Mg}$ [d] | 0.00 | 0.00 | 0.00 |
| $\Delta_{24}$ [e] | 0.07 | 0.08 | 0.03 |
| $C_m$ [f] | 0.13 | 0.13 | 0.08 |
| $C_\beta$ [f] | 0.36 | 0.35 | 0.31 |
| core size [b] | 2.072 | 2.080 | 2.073 |

[a] Average value in Å. [b] Value in Å. [c] Displacement (in Å) of magnesium from the 24-atom mean plane of the porphyrin core. [d] Displacement (in Å) of magnesium from the mean plane of the four pyrrole nitrogen atoms. [e] Average displacement (in Å) of the 24 atoms of the porphyrin macrocycle from the least-squares plane of the 24 atoms of the porphyrin ring. [f] Average displacement (in Å) from four porphyrinic nitrogen atoms.

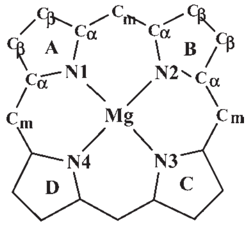

**Figure 2.** Formal diagram of the Mg(II) porphyrin core displaying the common symbol for MgTPP, MgTThP, and MgTFP; the corresponding independent bond lengths are summarized in Table 3.

The redox properties of three Mg(II) porphyrins were studied by cyclic voltammetric and differential pulse voltammetric techniques using tetrabutylammonium perchlorate as supporting electrolyte (0.1 M) in dichloromethane as solvent. A comparison of oxidation and reduction waves of cyclic voltammograms is shown in Figure 7, and data for all three Mg(II) porphyrin derivatives are presented in Table 5. In general, metalloporphyrins exhibit one or two ring centered oxidations and one or two ring centered reductions along with metal centered oxidation and reduction in case of redox active metal center present in the porphyrin cavity. But each of these three compounds exhibited only one ring-centered reduction (−1.40 V to −1.60 V) and one or two ring-centered oxidations (0.65 to 0.80 V). MgTPP and MgTThP exhibited two ring centered oxidations whereas MgTFP showed only one oxidation. The central metal Mg(II) being redox inactive did not show any metal centered oxidation or reduction. The oxidations and reductions were reversible or quasi-reversible ($\Delta E_p$ = 60−120 mV) except MgTFP which showed one irreversible oxidation. Inspection of the redox data (Table 5) reveals that the first oxidation potentials were shifted to more positive potential when six membered *meso*-phenyls were replaced with five membered *meso*-thienyl groups suggesting that MgTThP is harder to oxidize than MgTPP. However, the reduction potentials were shifted to less negative potential on replacement of *meso*-phenyl groups with *meso*-thienyl and *meso*-furyl groups indicating that the MgTThP and MgTFP are easier to reduce

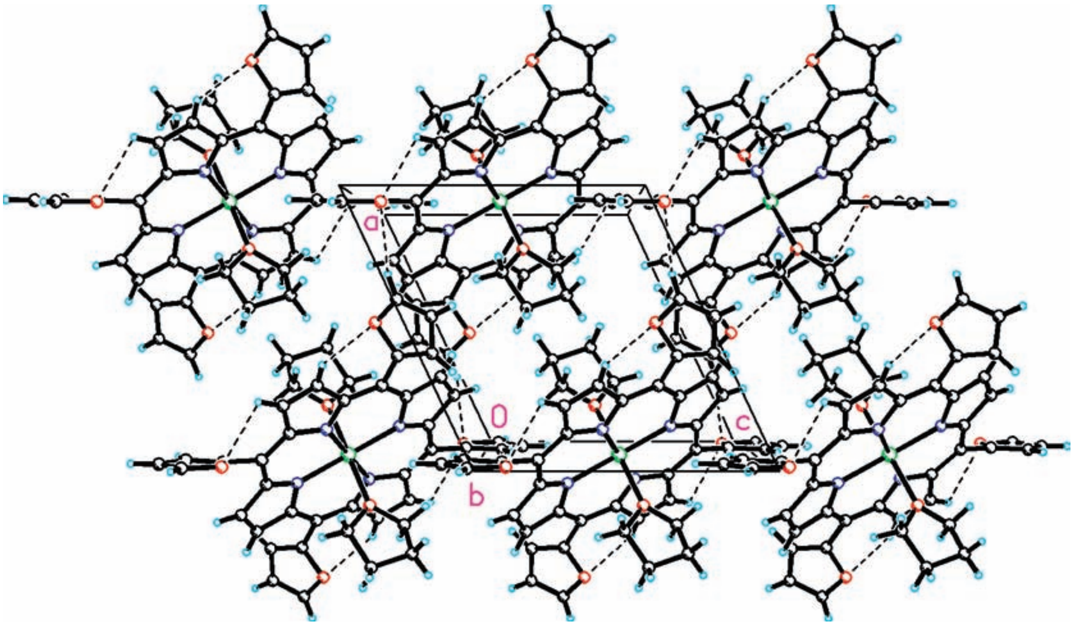

**Figure 3.** Molecular packing for compound MgTFP viewed down the *a* axis. The weak C−H····O intramolecular interactions between C−H of pyrrole ring and O of *meso*-furyl group are shown by dashed lines.

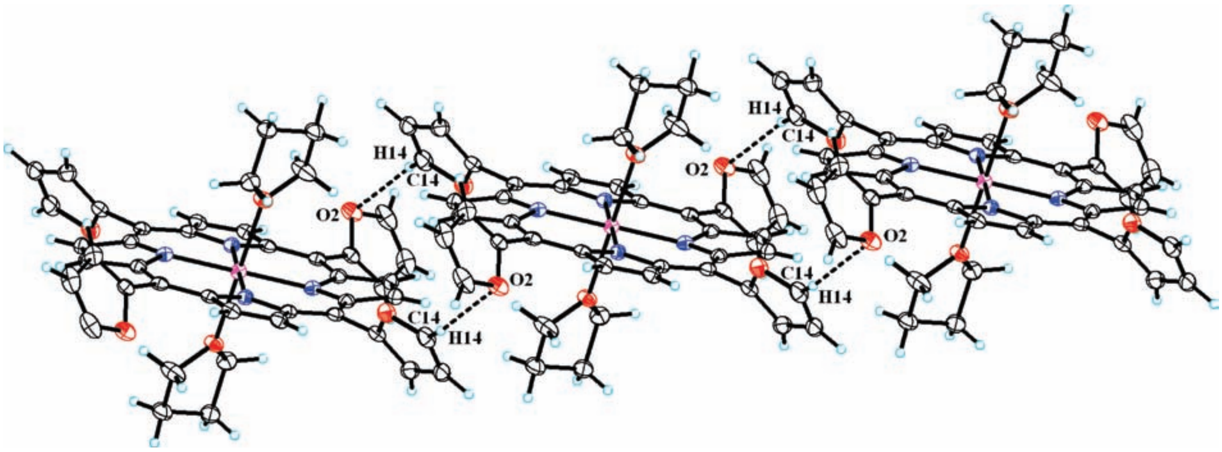

**Figure 4.** Supramolecular assembly through intermolecular-hydrogen bonding network (between O2····H−C14 and C14—H····O2 of *meso*-furyl group from two different porphyrin unit) in MgTFP complex.

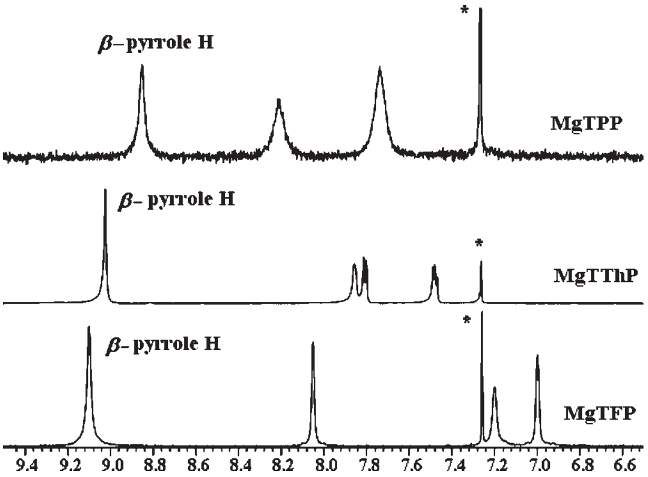

**Figure 5.** Comparison of $^1$H NMR of compounds MgTPP, MgTThP, and MgTFP (* = residual $CHCl_3$ in $CDCl_3$).

compared to MgTPP. Furthermore, the maximum anodic shifts for reduction potentials were observed for MgTFP suggesting that the MgTFP is easier to reduce than MgTThP.

The $\Delta_{redox}$ value which gives an estimate of HOMO−LUMO gap calculated from the difference of the first oxidation and first reduction potential is shown for MgTThP in Figure 8. The $\Delta_{redox}$ is decreased on changing *meso*-substituents from six membered phenyl groups to five membered thienyl groups (Table 5). The $\Delta_{redox}$ was not calculated for MgTFP since it exhibited an irreversible oxidation. The reduction of HOMO−LUMO gap explains the large red shifts of absorption bands of MgTThP compared to MgTPP. It is assumed that the HOMO−LUMO is further reduced in MgTFP which showed maximum red shifts in absorption bands compared to the other two Mg(II) porphyrins.

The fluorescence properties were studied by both steady state and time-resolved fluorescence techniques to understand the effect of *meso*-substituents on electronic properties of Mg(II) porphyrins in the singlet excited state. The comparison of fluorescence spectra is shown in Figure 9a, and the data are presented in Table 5. The MgTPP and MgTThP showed two fluorescence bands and MgTFP showed one broad fluorescence band. The inspection of Figure 9a and data presented in Table 5 reveal that the fluorescence bands experienced red shifts on changing *meso*-phenyl substituents to *meso*-thienyl and *meso*-furyl substituents, and maximum red shifts were observed for MgTFP. These observations are in line with the absorption studies and support the efficient $\pi$-delocalization between porphyrin and *meso*-substituents in MgTFP compared to MgTThP and MgTPP. The quantum yields calculated by comparative method showed the following trend: MgTPP > MgTFP > MgTThP. The low quantum yield of MgTThP was due to the presence of heavy sulfur atoms of *meso*-thienyl groups which enhances the non-radiative pathways and reduces the fluorescence yield. The singlet excited state lifetime was measured by single-photon counting technique. The Mg(II) porphyrins were excited at 406 nm, and emissions were detected at emission peak maxima of the corresponding Mg(II) porphyrin. The fluorescence decay of Mg(II) porphyrins was fitted to a single exponential, and the representative fluorescence decay profiles of MgTPP, MgTThP, and MgTFP along with residual fits are shown in Figure 9b and 9c, respectively. The singlet excited state lifetime $\tau_f$ of Mg(II) porphyrins is in agreement with their corresponding quantum yield, and the low singlet state lifetime observed for MgTThP is due to the presence of heavy sulfur atoms. Thus, the singlet state excited properties support the alteration of electronic properties on replacement of six membered *meso*-phenyl groups with five membered *meso*-thienyl and *meso*-furyl groups in Mg(II) porphyrins.

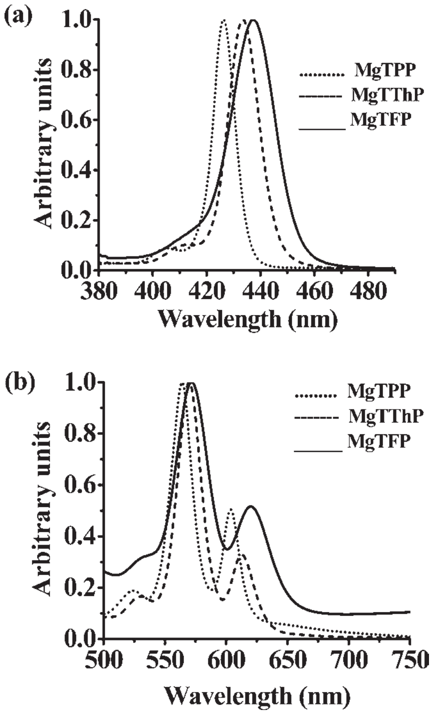

**Figure 6.** Comparison of normalized absorption spectra of MgTPP (dotted lines), MgTThP (dashed lines) and MgTFP (solid lines), recorded in toluene, (a) Soret band and (b) Q-band.

**Table 4.** $^1$H NMR Data and Absorption Data

| | $^1$H NMR [a] | absorption data [b] | |
|---|---|---|---|
| compound | $\delta$ in ppm $\beta$-pyrrole | Soret band $\lambda$ (nm) (log$\varepsilon$) | Q-bands $\lambda$ (nm) (log $\varepsilon$) |
| MgTPP | 8.85 (s, 8 H) | 426 (5.75) | 524 (sh), 564 (4.25), 604 (3.95) |
| MgTThP | 9.02 (s, 8 H) | 433 (5.74) | 530 (sh), 570 (4.28), 613 (3.79) |
| MgTFP | 9.10 (s, 8 H) | 437 (5.56) | 532 (sh), 572 (4.15), 620 (3.87) |

[a] All spectra recorded in $CDCl_3$. [b] All spectra recorded in toluene; the concentration used for Q-band spectra was ~5 × $10^{-5}$ M and for Soret band was ~5 × $10^{-7}$ M, sh = shoulder.

**Quantum Chemical Studies.** Minimum energy structures of three metalloporphyrins MgTPP, MgTThP, and MgTFP calculated at B3LYP/6-31G(d) level of theory are displayed in Figure 10. This choice of DFT functional and basis set should be adequate for metalloporphyrin systems. Selected bond lengths and torsion angles have been provided in Table 2 along with the X-ray crystallographic data for comparison. To bring about the direct correlation between calculated and experimentally observed properties, the equilibrium

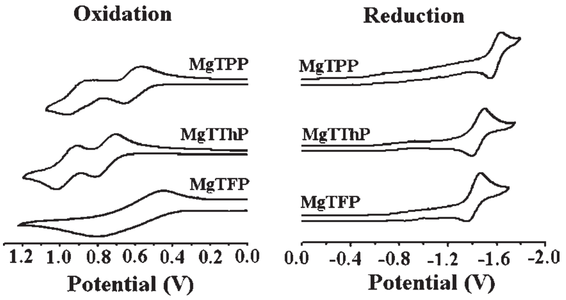

**Figure 7.** Comparison of oxidation and reduction waves of cyclic voltammograms (scan rate = 50 mV $s^{-1}$) of MgTPP, MgTThP, and MgTFP in $CH_2Cl_2$ containing 0.1 M tetrabutylammonium perchlorate (TBAP) as supporting electrolyte.

**Table 5.** Redox Potential Data and Emission Data

| | redox data [a] (V) | | | | emission data [b] | | | |
|---|---|---|---|---|---|---|---|---|
| | oxidation | | reduction | | | | | |
| compound | I | II | I | HOMO−LUMO gap ($\Delta_{redox}$) | Q (0, 0) (nm) | Q (0, 1) (nm) | $\Phi_f$ | $\tau_f$ (ns) |
| MgTPP | 0.65 | 0.94 | −1.57 | 2.22 | 609 | 660 | 0.16 | 8.90 |
| MgTThP | 0.78 | 0.98 | −1.42 | 2.20 | 626 | 669 | 0.003 | 0.37 |
| MgTFP | 0.68 [c] | | −1.40 | | 649 | | 0.024 | 3.28 |

[a] In $CH_2Cl_2$ solvent with 0.1 M tetrabutylammonium perchlorate (TBAP) as supporting electrolyte; scan rate = 50 mV $s^{-1}$. [b] All data were recorded in toluene. [c] Irreversible.

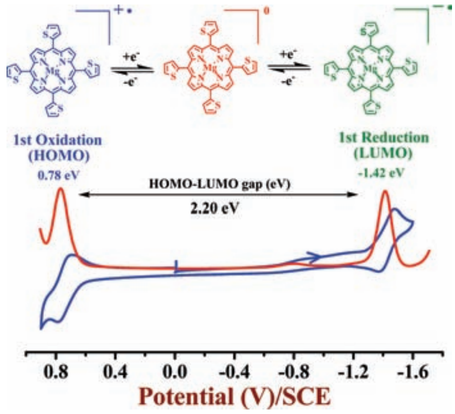

**Figure 8.** HOMO−LUMO gap of MgTThP.

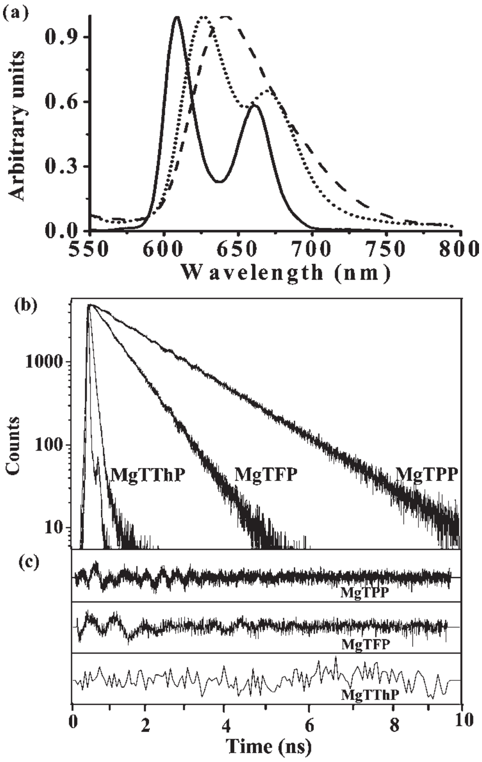

**Figure 9.** (a) Comparison of normalized emission spectra of MgTPP (solid lines), MgTThP (dotted lines), and MgTFP (dashed lines) recorded in toluene, (b) fluorescence decay profile, and (c) the weighted residuals distribution fit of fluorescence decays of MgTPP, MgTThP, and MgTFP. The excitation wavelength used was 406 nm, and emissions were detected at different wavelengths depending on the emission peak maxima of the corresponding *meso*-tetrasubstituted Mg(II) porphyrins.

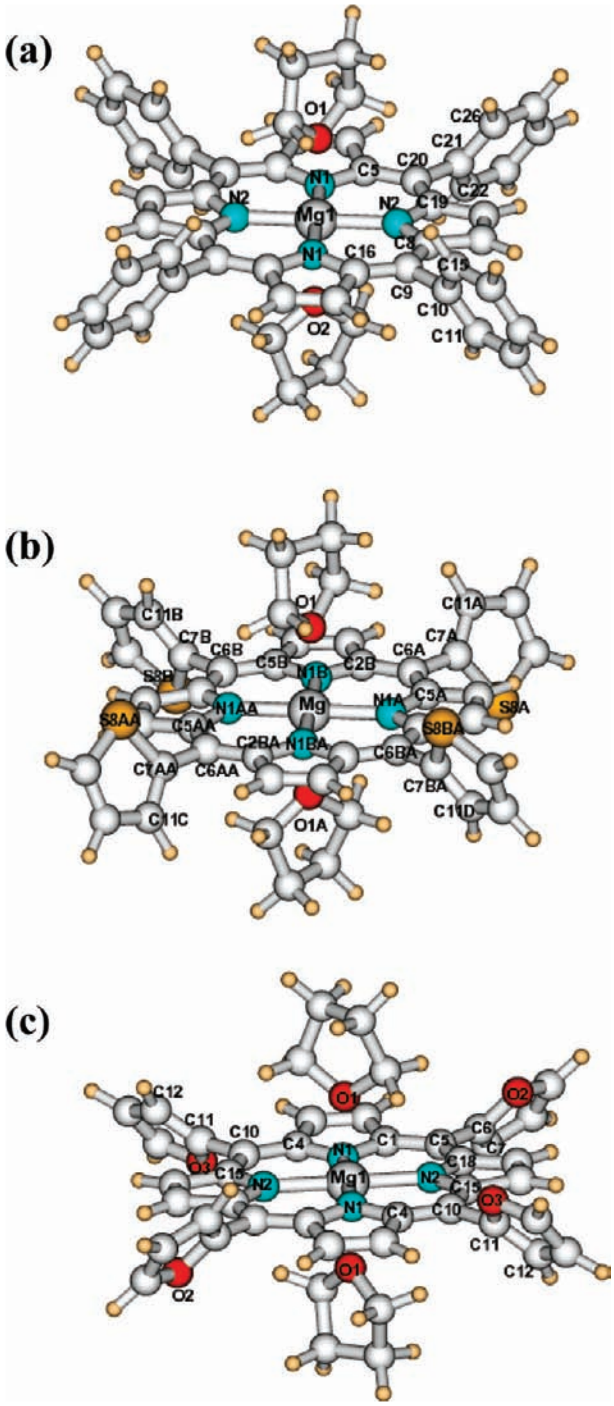

**Figure 10.** Fully optimized structures of (a) MgTPP, (b) MgTThP, and (c) MgTFP applying B3LYP/6-31G(d) level of theory (numbering of atoms for each complex has been shown following the corresponding crystal structure).

structures are optimized keeping two THF solvent molecules in the axial positions similar to crystal structures obtained for these Mg(II) porphyrins. It is observed that such geometrical arrangement leads to the most stable structure in the ground ($S_0$) state when full geometry optimization is carried out applying the Newton−Raphson procedure. The possibility of other conformers does exist, for example, in the case of MgTFP, the *meso*-furyl group can be arranged in all possible orientations with respect to the heteroatom oxygen because of possible allowed rotation through the single bond between the *meso*-carbon atom and the carbon atom through which *meso*-furyl group is attached to the porphyrin unit. In fact, a few optimizations are carried out taking such possible structures as the starting geometry which leads to a less stable structure. The cavity size of MgTPP and MgTThP is ~4.177 Å, and for MgTFP it is 4.188 Å. These values are close to the size obtained from crystal structure determination. The other parameters are also in line with crystallographically obtained data as displayed in Table 2. It is worth mentioning that theoretical calculations are carried out under isolated condition, and this leads to only one set of dihedral angles between *meso*-substituents and porphyrin plane in each case as there are no intermolecular interactions unlike in crystals. It is to be noted that the average dihedral angle between the *meso*-substituents and mean porphyrin ring are ~70° in MgTPP, and in MgTThP and ~53° in MgTFP. This indicates that *meso*-furyl group is more inclined toward porphyrin ring compared to *meso*-phenyl and *meso*-thienyl groups. Frontier molecular orbitals (FMO) are also calculated and displayed in Figure 11. This figure suggests more electronic delocalization in case of MgTFP, and the *meso*-furyl groups are involved in FMOs (HOMOs and LUMOs) to bring down the orbital energy through extensive $\pi$ conjugation. In the case of MgTPP, there is least involvement of *meso*-substituent orbitals in forming FMOs. The energies of HOMOs follow the order as MgTPP > MgTThP > MgTFP, and a similar trend is also observed in the case of the LUMO energy. This feature is clearly seen from the orbital correlation diagram as shown in Figure 11 with FMOs and corresponding energies of their respective porphyrin units. It is to be noted that neither the axial coordinating solvent molecule nor the central metal participates in either of the FMOs.

The FMO correlation diagram indicates that *meso*-substituents constitute a part of conjugated macrocycle showing $\pi$ overlap with the respective *meso*-substituents in both HOMOs and LUMOs. The energies of HOMOs for MgTPP, MgTThP, and MgTFP are −4.492 eV, −4.649 eV, and −4.764 eV, respectively. Similarly, the energies of LUMOs are −1.799 eV, −1.979 eV, and −2.237 eV for MgTPP, MgTThP, and MgTFP, respectively. By scrutinizing the energy values of the HOMO and LUMO of all three complexes, it is inferred that in the case of MgTFP, the HOMO and LUMO are stabilized by 0.115 and 0.258 eV, respectively, as compared to MgTThP. Similarly, in case of MgTThP, HOMO and LUMO are stabilized by 0.157 and 0.180 eV respectively relative to MgTPP. The HOMO−LUMO gaps calculated from these HOMO−LUMO energies follow the same trend (MgTPP > MgTThP > MgTFP) as obtained from cyclic voltammetry redox potential values. The substantial decrease of energy gap between HOMO and LUMO from MgTPP to MgTFP via MgTThP results in red shift in UV−vis spectra.

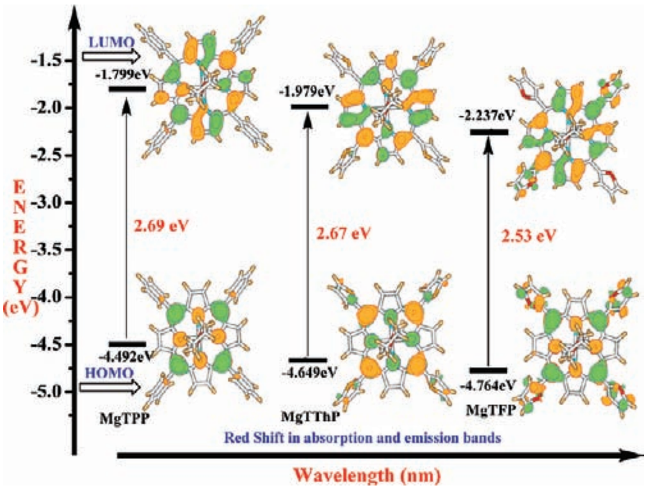

**Figure 11.** Orbital-correlation diagram of HOMO and LUMO (FMOs) for MgTPP, MgTThP, and MgTFP.

Vertical electronic transitions are calculated for these three metalloporphyrins applying the B3LYP functional under the TD-DFT formalism with the ground state ($S_0$) optimized structures predicted at the B3LYP level of theory. The COSMO model is also applied for accounting for the macroscopic solvent effect in the dichloromethane solvent. Results on a few low lying electronic transtions in the Soret band region are supplied in Table 6 showing the major electronic transitions involved in the observed Soret bands of these systems. As it is shown in Table 6, the strong electronic transitions having oscillator strength $f > 1.2$ are initiated from HOMO-1 orbital in all the three cases. Note that mainly pyrrole $\pi$ electrons have participated in the HOMO-1 orbital. The major electronic transitions occur to either LUMO or LUMO+1 orbital in all these systems. In both these molecular orbitals, mainly porphyrin ring $\pi^*$ electrons participate with a small contribution from one set of trans *meso*-substitutents. UV−vis spectra of these three metalloporphyrins in the Soret band region are simulated following a Gaussian model, and the spectra are depicted in Figure 12. The actual absorption maxima ($\lambda_{max}$) do not agree closely with calculated values. However, it is the order of values that is comparable.

## Conclusions

The influence of six membered versus five membered *meso*-substituents on structure, spectral, and redox properties of Mg(II) derivatives of *meso*-tetrasubstituted porphyrins was described using both experimental and theoretical approaches. The crystallographic study showed that the *meso*-furyl groups in MgTFP adopt a more in-plane arrangement with the porphyrin whereas the *meso*-phenyls in MgTPP and *meso*-thienyls in MgTThP are in out-of-plane arrangement with the porphyrin. This indicates that in MgTFP, there is a greater resonance interaction between *meso*-furyl groups and porphyrin ring leading to extension of $\pi$-conjugation whereas

**Table 6.** Vertical Transition Maxima (in nm) and Oscillator Strengths of Electronic Transitions in the Soret Band Region As Predicted by TD-DFT (B3LYP) Method Employing 6-31G(d) Basis Set in MgTPP, MgTThP and MgTFP

| system | dominant transitions | transition maxima (nm) | oscillator strengths |
|---|---|---|---|
| MgTPP | HOMO-1→LUMO+1 (49%), HOMO→LUMO (15%) | 402.5 | 1.3137 |
| | HOMO-1→LUMO (47%), HOMO→LUMO+1 (17%) | 401.9 | 1.3419 |
| | HOMO-3→LUMO (49%), HOMO-4→LUMO+1 (21%), HOMO-3→LUMO+1 (14%) | 349.4 | 0.0001 |
| MgTThP | HOMO-1→LUMO+1 (45%), HOMO→LUMO (17%) | 412.8 | 1.2487 |
| | HOMO-1→LUMO (44%), HOMO→LUMO+1 (18%) | 411.6 | 1.2656 |
| | HOMO-2→LUMO (51%), HOMO-2→LUMO+1 (33%) | 364.6 | 0.0001 |
| MgTFP | HOMO-1→LUMO+1 (36%), HOMO-1→LUMO (17%) | 421.4 | 1.2205 |
| | HOMO-1→LUMO (35%), HOMO-1→LUMO+1 (18%) | 420.0 | 1.2204 |
| | HOMO-2→LUMO (46%), HOMO-2→LUMO+1 (28%), HOMO-3→LUMO (13%) | 388.3 | 0.0000 |

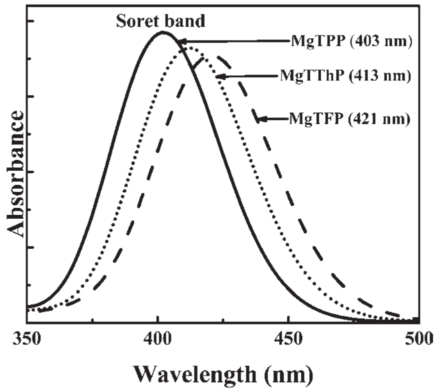

**Figure 12.** Simulated UV−vis spectra of MgTPP, MgTThP, and MgTFP in the Soret band region. Simulation of these absorption profiles was carried out from 10 low lying vertical excited states with Gaussian line shape.

in MgTPP and MgTThP, the interaction between *meso*-substituents and porphyrin ring is less. The DFT studies also support strong interaction between *meso*-substituents and porphyrin ring in MgTFP. The spectral and electrochemical studies are in agreement with the crystallographic studies. The absorption and fluorescence bands are shifted to the red on changing the *meso*-substituent from six membered phenyl groups to five membered thienyl and furyl groups, and maximum effects were observed for *meso*-tetrafuryl Mg(II) porphyrins. The electrochemical studies indicated a decrease of HOMO−LUMO gap on changing *meso*-substituents from six membered phenyl groups to five membered thienyl and furyl groups, and maximum decrease was noted for MgTFP which is in agreement with the large red shifts in absorption and fluorescence bands observed for MgTFP. Thus, it is concluded that by changing the *meso*-substituent from six membered aryl group to five membered aryl group, the electronic and structural properties of Mg(II) porphyrins can be tuned.

## Experimental Section

All general chemicals and solvents were procured from S.D. Fine Chemicals, India. Column chromatography was performed using silica gel and basic alumina obtained from Sisco Research Laboratories, India. $MgBr_2 \cdot O(Et)_2$ was purchased from Acros and used without further purifications. Tetrabutylammonium perchlorate was purchased from Fluka and used without further purifications.

$^1H$ NMR spectra were recorded with Varian 400 MHz instrument using tetramethylsilane as an internal standard. All NMR measurements were carried out at room temperature in deuterochloroform. Absorption and steady state fluorescence spectra were obtained with Perkin−Elmer Lambda-35 and Lambda-55 instruments, respectively. The fluorescence quantum yields ($\Phi_f$) of Mg(II) porphyrins were estimated from the emission and absorption spectra by comparative method.[16] ES-MS spectra were recorded with a Q-Tof Micromass spectrometer. Cyclic voltammetric (CV) and differential pulse voltammetric (DPV) studies were carried out with BAS electrochemical system utilizing the three electrode configuration consisting of a glassy carbon (working electrode), platinum wire (auxiliary electrode), and saturated calomel (reference electrode) electrodes in dry dichloromethane using 0.1 M tetrabutylammonium perchlorate as supporting electrolyte.

**X-ray Crystallography.** Suitable single crystals were grown by slow diffusion of *n*-hexane into the THF solution of corresponding Mg(II)porphyrins. Single crystal X-ray structural studies of MgTPP and MgTFP were performed on a CCD Oxford Diffraction XCALIBUR-S diffractometer equipped with an Oxford Instruments low-temperature attachment. Data were collected at 293(2) K (in case of MgTPP) and 120(2) K (in case of MgTFP) using graphite-monochromoated Mo Kα radiation ($\lambda_\alpha = 0.71073$ Å). The strategy for the data collection was evaluated by using the CrysAlisPro CCD software. The data were collected by the standard $\varphi$-$\omega$ scan techniques, and were scaled and reduced using the CrysAlisPro RED software. The structures were solved by the direct method using SHELXS-97[17] and refined by full matrix least-squares with SHELXL-97, refining on $F^2$. The positions of all the atoms were obtained by direct method. All non-hydrogen atoms were refined anisotropically. The hydrogen atoms were placed in geometrically constrained positions and refined with isotropic temperature factor, generally $1.2U_{eq}$ of their parent atoms. The data set for complex MgTThP was collected with a Nonius KappaCCD diffractometer, equipped with a rotating anode generator at 223(2) K. Programs used: data collection COLLECT (Nonius B.V., 1998), data reduction Denzo-SMN,[18] absorption correction Denzo,[19] structure solution SHELXS-97,[20] structure refinement SHELXL-97,[17] graphics SCHAKAL (E. Keller, 1997).

In the case of MgTPP one of the carbon atoms (C3) of the axial THF was disordered over two conformations with occupancy factors of 0.64(1) and 0.36(1). In MgTThP both independent thiophene molecules in the asymmetric unit are disordered, they were refined with split positions to resulting occupancies of 0.896(3):0.104(3) and 0.646(2):0.354(2), respectively. Geometrical (SAME = same geometry, SAME is used as a relative weak restraint making all bond lengths in two parts of a molecule equal within a given standard deviation), and thermal (EADP = equal anisotropic displacement parameters) restraints were applied for the minor components.

**Theoretical Methods.** DFT calculations were carried out on three Mg(II) porphyrin systems, namely, MgTPP, MgTThP, and MgTFP to find out minimum energy structures and to study their electronic properties. Searches for these structures were performed in the ground electronic state ($S_0$) applying Becke's three parameters correlated hybrid density functional, B3LYP adopting 6-31G(d) atomic basis functions which includes at least 3200 primitive Gaussian functions in total. Equilibrium structures of these systems were calculated based on full geometry optimization following the Newton−Raphson procedure. Excited state calculations were carried out applying the TD-DFT procedure with the B3LYP functional for 10 low lying vertical electronic transitions on the $S_0$ state optimized structure using the COSMO solvation model to account for the solvent ($CH_2Cl_2$) effect with the same set of basis functions. Simulation of absorption profiles was carried out from 10 low lying excited states with Gaussian line shape, that is,

$$\varepsilon(E) = A\sum_i \frac{f_i}{\Delta_i} \exp\left(B\frac{(E-E_i)^2}{\Delta_i^2}\right)$$

where, ε, E, f, Δ are molar extinction coefficient, transition energy, oscillator strength, and half bandwidth, respectively. UV−vis spectra were generated by considering the full-width at half-maximum (fwhm) as 100 nm. The total integrated intensity under the absorption profile was kept equal to the sum of all the

---

[16] Gupta, I.; Ravikanth, M. *Inorg. Chem. Acta* **2007**, *360*, 1731–1742.

[17] Sheldrick, G. M. *Acta Crystallogr.* **2008**, *A64*, 112−122; SHELX, Program for Crystal Structure Solution and Refinement, University of Goettingen, Germany, **1997**.

[18] Otwinowski, Z.; Minor, W. *Methods Enzymol.* **1997**, *276*, 307–326.

[19] Otwinowski, Z.; Borek, D.; Majewski, W.; Minor, W. *Acta Crystallogr.* **2003**, *A59*, 228–234.

[20] Sheldrick, G. M. *Acta Crystallogr.* **1990**, *A46*, 467–473.

oscillator strengths. All the electronic structure calculations were carried out applying GAMESS suite of ab initio program.[21] Visualization of molecular structures and orbital contour plots were carried out using the Molden visualization software.[22]

**General Synthesis.** The magnesium complexes of porphyrins were prepared according to literature procedure. There are several methods available for magnesium insertion into the porphyrin cavity. We followed the most useful Lindsey's method[8a] which produces the desired complexes in very good yield in case of MgTPP and MgTFP. But to synthesize MgTThP, we had to follow conventional route where $H_2$TThP and $MgCl_2$ were refluxed in DMF.[7]

**Synthesis of Mg$^{II}$ Derivatives of TPP, TThP and TFP. MgTPP Complex.** MgTPP was synthesized by following Lindsey's method[8a] reported in literature. Mp > 300 °C. $^1$H NMR (400 MHz, $CDCl_3$, 298 K): $\delta$ 8.85 (s, 8H, $\beta$-pyrrole), 8.21 (br s, 8H, *o*-H, *meso*-phenyl), 7.74 (br s, 12 H, *m*-, *p*-H, *meso*-phenyl) ppm. ES-MS: $C_{44}H_{28}N_4Mg$ calcd avg mass 636.2, obsd *m*/*z* 637.2 $[M+1]^+$.

**MgTThP Complex.** A sample of 100 mg (0.157 mmol) of $H_2$TThP was dissolved in 100 mL of DMF in a one-neck round-bottom flask. Then 320 mg (1.57 mmol) of $MgCl_2 \cdot 6H_2O$ was added into that solution. The mixture was then refluxed overnight. The solution became greenish pink in color. The solvent was removed completely to dryness under reduced pressure. The solid obtained was loaded onto an alumina column packed in $CH_2Cl_2$ containing 0.1% triethylamine and eluted with $CH_2C1_2$ to remove the residual $H_2$TThP. Elution with $CH_2Cl_2$/acetone (1: 1) afforded the desired MgTThP as dark blue solid in 91% yield (94 mg). Mp > 300 °C. $^1$H NMR (400 MHz, $CDCl_3$, 298 K): $\delta$ 9.02 (s, 8H, $\beta$-pyrrole), 7.85 (br s, 4H, α-H, *meso*-thienyl), 7.80 (d, 4H, $\beta$-H, *meso*-thienyl), 7.44−7.49 (m, 4H, $\beta$-H, *meso*-thienyl) ppm. ES-MS: $C_{36}H_{20}N_4S_4Mg$ calcd avg mass 660.1, obsd *m*/*z* 661.3 $[M+1]^+$.

**MgTFP Complex.** A 100 mg portion (0.174 mmol) of $H_2$TFP was dissolved in 8 mL of $CH_2C1_2$ in a one-neck round-bottom flask. Then 0.485 mL (3.48 mmol) of triethylamine was added followed by 449 mg (1.74 mmol) of $MgBr_2 \cdot O(Et)_2$. The reaction mixture was stirred magnetically at room temperature for 15 min. The progress of complete metalation was judged by absorption spectroscopy. Then about 25 mL of $CH_2C1_2$ was added into the reaction mixture, washed with 5% $NaHCO_3$, dried (over $Na_2SO_4$), and filtered, and the filtrate was concentrated to 4−5 mL. Chromatography on an alumina column (packed in $CH_2Cl_2$ containing 0.1% triethylamine) with $CH_2C1_2$ elution yielded unreacted $H_2$TFP. Repeat column chromatography always yields some free base $H_2$TFP. Desired compound was collected as a purple-green fraction by elution with $CH_2Cl_2$/acetone (1: 1). These fractions were evaporated to dryness, and the crude solid compound was recrystallized with *n*-hexanes affording dark green solid. Yields: 96 mg (93%). Mp > 300 °C. $^1$H NMR (400 MHz, $CDCl_3$, 298 K): $\delta$ 9.10 (s, 8H, $\beta$-pyrrole), 8.05(s, 4H, α-H, *meso*-furyl), 7.20 (br s, 4H, $\beta$-H, *meso*-furyl), 7.00 (br s, 4H, $\beta$-H, *meso*-furyl) ppm. ES-MS: $C_{36}H_{20}N_4O_4Mg$ calcd avg mass 596.1, obsd *m*/*z* 597.2 $[M+1]^+$.

**Acknowledgment.** M.R. thanks CSIR and DST for financial support, and A.G. thanks IIT-Bombay for a fellowship. Computer Centre, BARC is gratefully acknowledged for generous CPU time in ANUPAM parallel computer systems. Authors also thank Mr. Ranjan Patra for his help.

---

(21) Schmidt, M. W.; Baldridge, K. K.; Boatz, J. A.; Elbert, S. T.; Gordon, M. S.; Jensen, J. H.; Koseki, S.; Matsunaga, N.; Nguyen, K. A.; Su, S. J.; Windus, T. L.; Dupuis, M.; Montgomery, J. A. *J. Comput. Chem.* **1993**, *14*, 1347–1363.

(22) Schaftenaar, G.; Noordik, J. H. *J. Comput.-Aided Mol. Des.* **2000**, *14*, 123–134.